Macromolecular Rapid Communications
www.mrc-journal.de

Optothermally Reversible Carbon Nanotube–DNA Supramolecular Hybrid Hydrogels

*Nikhita D. Mansukhani, Linda M. Guiney, Zonghui Wei, Eric W. Roth, Karl W. Putz, Erik Luijten, and Mark C. Hersam**

Supramolecular hydrogels (SMHs) are three-dimensional constructs wherein the majority of the volume is occupied by water. Since the bonding forces between the components of SMHs are noncovalent, SMH properties are often tunable, stimuli-responsive, and reversible, which enables applications including triggered drug release, sensing, and tissue engineering. Meanwhile, single-walled carbon nanotubes (SWCNTs) possess superlative electrical and thermal conductivities, high mechanical strength, and strong optical absorption at near-infrared wavelengths that have the potential to add unique functionality to SMHs. However, SWCNT-based SMHs have thus far not realized the potential of the optical properties of SWCNTs to enable reversible response to near-infrared irradiation. Here, we present a novel SMH architecture comprised solely of DNA and SWCNTs, wherein noncovalent interactions provide structural integrity without compromising the intrinsic properties of SWCNTs. The mechanical properties of these SMHs are readily tuned by varying the relative concentrations of DNA and SWCNTs, which varies the cross-linking density as shown by molecular dynamics simulations. Moreover, the SMH gelation transition is fully reversible and can be triggered by a change in temperature or near-infrared irradiation. This work explores a new regime for SMHs with potential utility for a range of applications including sensors, actuators, responsive substrates, and 3D printing.

1. Introduction

Hydrogels have attracted wide interest for a variety of mechanical, biomedical, and chemical applications.[1] They are typically based on covalently cross-linked hydrophilic polymers, and have the ability to swell by absorbing and retaining large amounts of water. Supramolecular hydrogels (SMHs), by contrast, employ molecular subunits along with biomolecules and functionalized nanoparticles, which are cross-linked by noncovalent forces such as electrostatic interactions, hydrogen bonding, metal–ligand bonding, or host–guest chemistry.[2] Noncovalent cross-linking forces are relatively weak and therefore dynamic, resulting in constructs that are highly adaptable, tunable, and stimuli-responsive. Consequently, SMHs have received significant attention for applications such as self-healing, sensing, and cell encapsulation.[3]

Single-walled carbon nanotubes (SWCNTs) are well known for their extraordinary physical, optical, and electronic properties.[4] For example, their 1D nature leads to van Hove singularities in the density of states that imply strong peaks in SWCNT optical absorption spectra. For common semiconducting SWCNTs, these optical absorption peaks occur at near-infrared (NIR) wavelengths, which fall in the transparency window for biological tissue.[5] Since SWCNTs are hydrophobic, surface functionalization is necessary to form dispersions in aqueous solutions. While covalent surface modification compromises the intrinsic optical properties of SWCNTs, noncovalent functionalization (e.g., using amphiphilic surfactants, synthetic polymers, or biomolecules such as DNA) preserves the original SWCNT sp^2-bonding and thus the SWCNT optical properties remain intact.[6]

N. D. Mansukhani, L. M. Guiney, E. W. Roth, Dr. K. W. Putz, Prof. E. Luijten, Prof. M. C. Hersam
Department of Materials Science and Engineering
Northwestern University
2220 Campus Drive, Evanston, IL 60208, USA
E-mail: m-hersam@northwestern.edu

Z. Wei, Prof. E. Luijten, Prof. M. C. Hersam
Applied Physics Graduate Program
Northwestern University
2145 Sheridan Road, Evanston, IL 60208, USA

The ORCID identification number(s) for the author(s) of this article can be found under https://doi.org/10.1002/marc.201700587.

DOI: 10.1002/marc.201700587

Prof. E. Luijten
Department of Engineering Sciences and Applied Mathematics
Northwestern University
2145 Sheridan Road, Evanston, IL 60208, USA

Prof. E. Luijten
Department of Physics and Astronomy
Northwestern University
2145 Sheridan Road, Evanston, IL 60208, USA

Prof. M. C. Hersam
Department of Chemistry
Northwestern University
2145 Sheridan Road, Evanston, IL 60208, USA

Prof. M. C. Hersam
Department of Electrical Engineering and Computer Science
Northwestern University
2145 Sheridan Road, Evanston, IL 60208, USA

In an effort to unite the desirable attributes of SMHs and SWCNTs, several reports have explored the incorporation of SWCNTs in hydrogel and SMH constructs. In traditional hydrogels, SWCNTs have provided mechanical reinforcement and stimuli-responsive properties such as a mechanical response upon exposure to NIR irradiation.[7] In the high concentration limit, SWCNTs have themselves formed gels without additives through van der Waals bonding.[8] In addition, since SWCNTs can form complexes with a variety of macromolecules, they have been incorporated into SMHs in conjunction with polymers, polysaccharides, DNA, and other biomolecules.[9] However, although some degree of thermal, chemical, and optical responsiveness has been achieved in SWCNT-based SMHs, reversible responses to NIR irradiation are noticeably absent from prior reports.[10]

Here, we present a novel SMH architecture comprised only of DNA and SWCNTs that employs DNA base pairing as the cross-linking interaction. This SWCNT-DNA SMH design allows highly tunable mechanical properties as a function of the relative concentration of SWCNTs and DNA. Furthermore, by varying the DNA sequence length, SWCNT-DNA SMH stability can be engineered, ultimately allowing robust structures across biologically relevant ranges of pH. The observed properties are consistent with molecular dynamics simulations that relate cross-linking density to SWCNT concentration and DNA sequence length. Finally, we demonstrate full thermal and optical reversibility of the SWCNT-DNA SMHs as a function of temperature or NIR optical irradiation. The properties of these SWCNT-DNA SMHs hold promise for a range of applications including substrate-responsive materials, sensing, and 3D printing.[11]

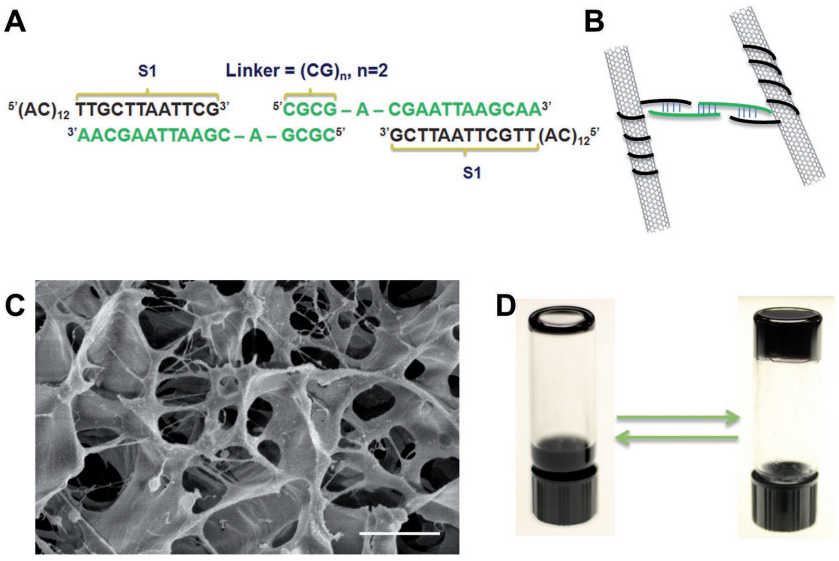

Figure 1. Schematic and physical characterization of the SWCNT-DNA SMH structure. A) DNA sequence $(AC)_{12}S1$ (black) is used to disperse SWCNTs. The linker DNA (green) has two regions: one complementary to S1 to hybridize with the SWCNT and one self-complementary (CG) repeat of variable length, separated by a single adenosine base. B) Proposed structure upon gel formation, wherein $(AC)_{12}S1$ helically wraps around the SWCNT while the linker DNA forms duplexes with both S1 and other linker strands, thereby providing the cross-linking mechanism. C) Cryo-SEM of a lyophilized SWCNT-DNA gel, showing a network of SWCNTs amid aggregated buffer salts and DNA. D) Photographs of the inverted-vial test to demonstrate the sol-gel transition (solution on left and gel on right).

2. Results and Discussion

Drawing inspiration from DNA-modified gold nanoparticle assembly and DNA hydrogels, our SMH design utilizes only SWCNTs and DNA.[12] SWCNTs are first dispersed in aqueous solution with single-stranded DNA consisting of 12 adenosine-cytosine (AC) repeats attached to an 12-base pair sequence called "S1," labeled "$(AC)_{12}S1$," as shown in **Figure 1**A,B (see the Experimental Section for further details). This DNA sequence is chosen for its lack of hairpin formation and for the strong affinity of AC bases for SWCNTs.[13] (6,5) SWCNTs are chosen for their widespread availability in purified form and strong absorption in the NIR range. The dispersion is formed in aqueous buffer solution consisting of 4-(2-hydroxyethyl)-1-piperazineethanesulfonic acid (HEPES), potassium acetate, and sodium chloride with pH 7.5. The resulting dispersion is characterized by optical absorbance spectroscopy (Figure S1, Supporting Information) and then exposed to an excess of linker DNA, also shown in Figure 1A,B. The linker DNA strands are comprised of two regions: a region that is complementary to the SWCNT-adsorbed DNA (sequence S1), and another region of (CG) repeats of variable length. Between the two regions is a single adenosine (A) base that enhances the flexibility of the linker.[12] The CG region is self-complementary and can form a duplex with other SWCNT-bound linker DNA strands, thereby providing the basis for a DNA cross-linked network of SWCNTs. Indeed, upon addition of excess linker DNA and a slow annealing step, a SWCNT-DNA SMH is formed. Figure 1C contains a cryo-SEM (scanning electron microscopy) image of a lyophilized SWCNT-DNA SMH following slow freeze etching, thereby allowing visualization of the SWCNT network, while Figure 1D demonstrates the sol-gel transition.

To verify the proposed gelation mechanism, the rheology of the SWCNT-DNA SMH is compared in the presence and absence of linker DNA. These experiments determine the necessity of the DNA linker in addition to the base-pair specificity of linker cross-linking. In these rheological studies, strain sweeps are used to determine the storage (G') and loss (G'') moduli (**Figure 2**A). A representative shear stress sweep shows that the viscosity of a typical 1.8 mg mL^{-1} SWCNT-DNA SMH is 900 Pa s (Figure 2B). The preparation of SWCNT-DNA dispersions with a noncomplementary linker or a lack of linker does not result in gel formation, supporting our hypothesis that the duplex linker is formed (Figure S2, Supporting Information). Furthermore, we compare our SWCNT-DNA SMH to SWCNT-DNA gels that are known to form through van der Waals interactions at high concentrations. Without the linker present, our SWCNT-DNA dispersions form a van der Waals gel at

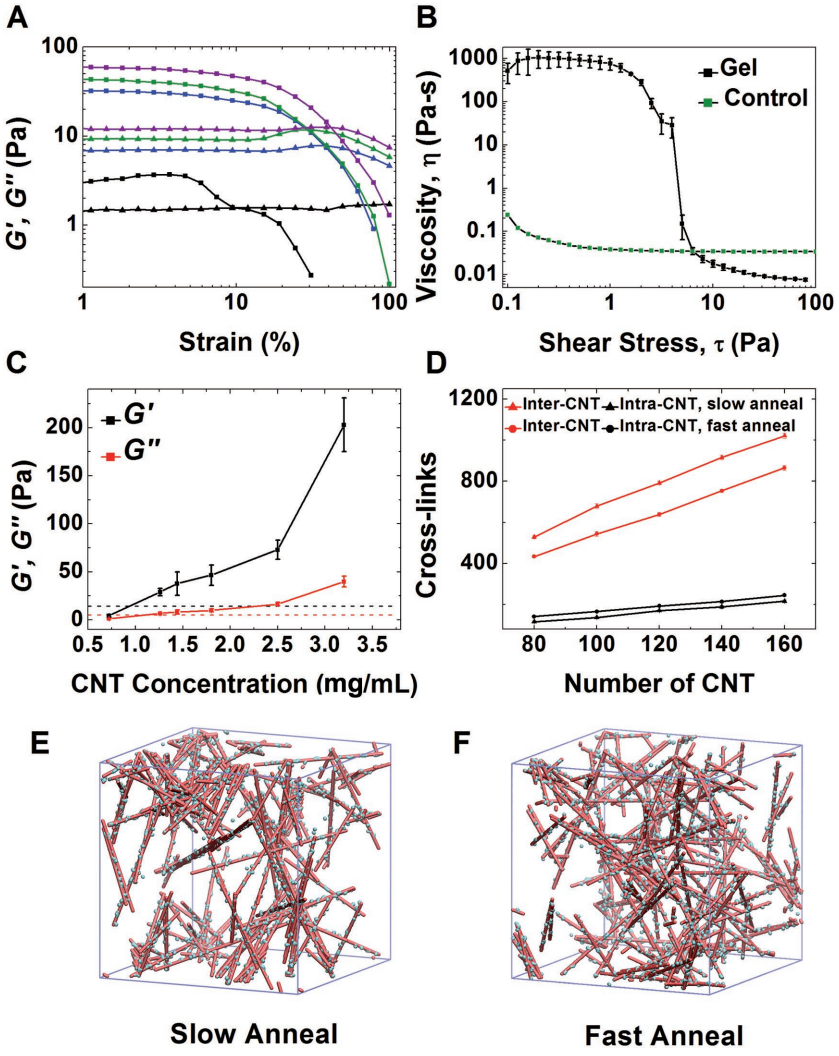

Figure 2. Tunable mechanical properties based on the concentration of SWCNTs. A) Strain sweeps of several representative samples. Squares represent G'; triangles represent G''. Purple, green, blue, and black spectra represent gels with SWCNT concentrations of 1.8, 1.44, 1.25, and 0.72 mg mL^{-1}, respectively. B) Viscosity versus shear stress for a typical gel, compared to an ungelled sample. C) Storage (G') and loss (G'') moduli as a function of SWCNT concentration. Linker DNA concentration is increased in proportion to SWCNT concentration. Dashed black and red lines indicate moduli for a 5 mg mL^{-1} van der Waals gel. D) Number of inter-SWCNT and intra-SWCNT cross-links in simulation, as a function of the number of SWCNTs for gel systems formed at slow and fast annealing rates. E,F) Representative simulation configuration of gels formed by 100 SWCNTs at slow and fast annealing rates. SWCNTs are shown in pink. S1 strand and linker DNA are both shown in cyan.

SWCNT concentrations above 5 mg mL^{-1}. However, in the presence of the linker, gelation occurs at a SWCNT concentration as low as 1.25 mg mL^{-1}. In addition, the DNA cross-linked SWCNT gel at a SWCNT loading of 1.8 mg mL^{-1} is found to have a G' of 46 Pa, whereas the 5 mg mL^{-1} van der Waals gel has a G' of only 15 Pa, indicating that DNA base-pairing contributes to mechanical strength and integrity.

The mechanical properties of the SWCNT-DNA SMHs can also be tuned by varying the SWCNT concentration. At concentrations lower than that of the van der Waals gel, the storage modulus of the gels strongly depends on the SWCNT concentration, with a measured value as large as 200 Pa at a SWCNT concentration of 3.2 mg mL^{-1} (Figure 2C). The presence of linker DNA is increased proportionally to the SWCNT concentration at a 1:1 ratio. To facilitate a deeper understanding of the SWCNT-DNA SMH structure and to explore the dependence of cross-linking density on SWCNT concentration, molecular dynamics (MD) simulations were carried out using a coarse-grained model. In particular, the SWCNTs are represented by a rigid linear array of beads, as detailed in the Experimental Section. The S1 strand and the $(CG)_n$ strand of linker DNA are modeled using a bead-spring polymer model. For simplicity, this model assumes that the $(AC)_{12}$ strand of the DNA that strongly interacts with the SWCNT surface has a negligible contribution to cross-linking and thus can be represented by a direct bond of the S1 strand to one of the SWCNT beads (Figure S3, Supporting Information). Given the small Debye length of ≈0.3 nm at the salt concentration employed in the experiments, electrostatic interactions are ignored in the simulations. Instead, all components are assumed to interact with each other through excluded-volume interactions, which are modeled via shifted-truncated Lennard–Jones (LJ) potentials. The formation of cross-links is simulated via a dynamic bonding function. Additional modeling details are provided in the Supporting Information.

In the simulations, we emulate the heating and subsequent cooling of the mixture of DNA-dispersed SWCNTs and linker DNA that is present during gel synthesis (see the Experimental Section). Since the simulation employs coarse-grained building blocks, the corresponding effective annealing rate must be determined empirically. To this end, we first simulate six systems with different annealing rates and compare the configurations and the number of cross-links in the formed gel. Simulation results (Figure S4, Supporting Information) show that the number of cross-links increases as the annealing rate decreases, and that the slowest annealing rate (Rate 1) results in strong SWCNT aggregation with a large number of inter-SWCNT cross-links. Given that the gel synthesized in the experiments is homogeneous, we conclude that the appropriate annealing rate in simulation must be faster. On the other hand, it must be slower than Rate 6, which corresponds to an immediate quench to room temperature.

To investigate the impact of SWCNT concentration on the gel cross-linking density, the system is simulated at two representative annealing rates: the "slow" and "fast" rates corresponding to Rates 3 and 5 in Figure S4 (Supporting Information), respectively. Figure 2E,F, respectively, shows representative configurations of the gel formed by 100

SWCNTs at these two annealing rates, where SWCNTs are shown in pink and the DNA strands (S1 and linker) are shown in cyan. Figure 2D shows the total number of cross-links as a function of the number of SWCNTs. For both annealing rates, the number of inter-SWCNT cross-links increases linearly with SWCNT concentration. The inter-SWCNT cross-links contribute to the mechanical strength of the gel, as reflected by the corresponding increase in the modulus of the gel (Figure 2C). At the slow annealing rate, the SWCNTs tend to be more aligned with each other (Figure 2E), leading to a larger number of inter-SWCNT cross-links. Besides the inter-SWCNT cross-links, nearby S1 strands can form intra-SWCNT cross-links in the presence of linker DNA. The number of intra-SWCNT cross-links also increases linearly with increasing SWCNT concentration. However, the gel formed at the slower annealing rate has a slightly reduced number of intra-SWCNT cross-links.

The length of the linker DNA and the pH of the buffer are also varied to determine their effects on the mechanical and melting properties of the gel. Specifically, we vary the pH from 6 to 10, and the number of repeat units of the $(CG)_n$ region of the linker DNA from n = 2 to 9 (or 4 to 18 bases). As n increases, the moduli G' and G'' decrease slowly, indicating a weakening but enduring gel structure (**Figure 3**A). Since the inter-SWCNT cross-linking density is closely related to mechanical strength, MD simulations are again employed to explore the effect of linker length on cross-linking density. In these simulations, the linker length is varied from 1 to 6 beads (with bead diameter 1 nm), corresponding to a linker $(CG)_n$ region length ranging from 4 to 18 bases in the experimental setup. Figure 3B,C shows the number of inter-SWCNT and intra-SWCNT cross-links as well as free S1 strands (including those that may connect to linker DNA but do not form cross-links) as a function of linker length for different annealing rates. As linker length increases, the probability of nearby S1 strands forming an intra-SWCNT cross-link is enhanced. The competing formation of intra-SWCNT cross-links reduces the overall number of inter-SWCNT cross-links and free S1 strands, as demonstrated in Figure 3B,C for gel systems formed at fast and slow annealing rates. The reduced number of inter-SWCNT cross-links in turn contributes to the decrease of G' at longer linker length (Figure 3A).

In the rheological measurements, the melting temperature (i.e., the gel-sol transition point) is defined as the temperature at which G' drops below G'', thereby no longer meeting the rheological standard for a solid material. Keeping S1 constant, we expect some increase in the melting temperature of the gel as n is increased from 4 to 9, and indeed a rise in the melting temperature is observed from 42 to 52 °C (Figure 3D). DNA duplex stability can be predicted from the base sequence.[14] Specifically, the temperature at which complementary strands in the 5′-$(CG)_n$-3′ duplex dissociate increases with n, consistent with the experimental observation that the gel melting temperature increases with increasing linker length. The measured gel melting temperature is well below the dissociation temperatures of free 5′-$(CG)_n$-3′ and free S1 duplexes in solution, which are above 86 °C. This observation can be understood from the fact that a fraction of cross-links will break below the DNA dissociation temperature, thereby melting the gel. Since pH

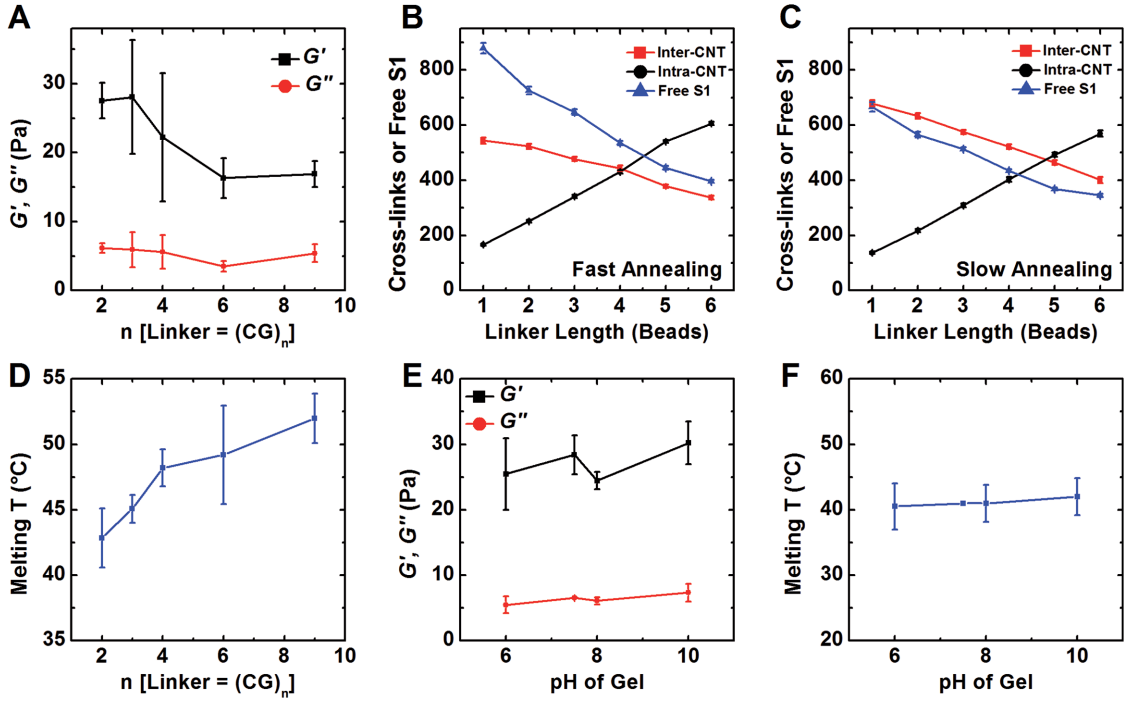

Figure 3. Mechanical properties and melting temperature as a function of linker length and pH. A) G' and G'' as a function of linker length, showing a gradual weakening of the mechanical properties. The number of inter-SWCNT and intra-SWCNT cross-links as well as the number of free S1 strands as a function of linker length for gel systems formed in MD simulations at B) fast and C) slow annealing rates. D) SWCNT-DNA SMH melting temperatures increase with DNA linker length due to enhanced cross-linking stability. SWCNT-DNA SMH melting temperatures are lower than free duplexes in solution. SWCNT-DNA SMH E) mechanical properties and F) melting temperature remain stable for pH values in the range 6–10.

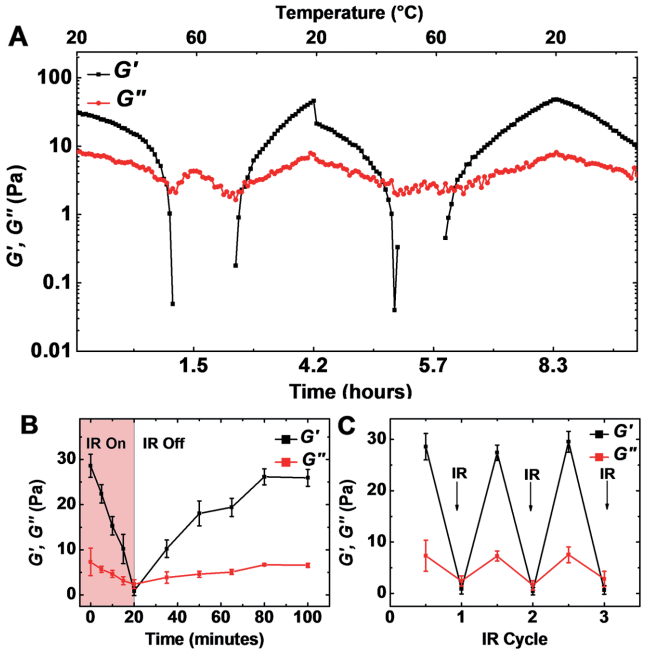

Figure 4. Optothermal reversibility of SWCNT-DNA SMHs. A) Temperature is cycled between 20 and 60 °C while the SWCNT-DNA SMH is constantly measured. The crossover between *G′* and *G″* marks the reversible sol-gel transition. B) NIR light drives the gel-sol transition after 20 min of irradiation. After irradiation, the SMH recovers to its original rheological state within 60 min. C) NIR reversibility is shown by repeated cycles of irradiation and recovery of the SWCNT-DNA SMH.

is an important factor in many applications of hydrogels, its effect on SWCNT-DNA SMHs was also examined. Figure 3E,F shows that the mechanical properties and melting temperature of the gel are unaffected for pH values in the range of 6–10 (Figure 3E,F). Below pH 6, the SWCNT-DNA dispersions are destabilized, most likely due to the disruption of SWCNT-DNA interactions at low pH. Above pH 10, gels do not form, presumably due to the disruption of DNA base pairing at high pH.

Finally, the optothermal reversibility of SWCNT-DNA SMHs are explored rheologically. By measuring the crossover point of *G′* and *G″*, we effectively record repeated gel-sol and sol-gel transitions. Thermoreversibility was demonstrated by cycling the ambient and plate temperature in the rheometer between 20 and 60 °C. The gel readily cycles between a sol and gel state in response to cyclic temperature changes (**Figure 4**A). Moreover, the SWCNTs absorb NIR light leading to local heating that provides another means of sol-gel triggering. In Figure 4B, SWCNT-DNA SMHs are irradiated with 976 nm light, during which time the crossover between *G′* and *G″* is observed after 20 min. Following irradiation, the NIR light source is turned off, and the SWCNT-DNA SMHs spontaneously recover to their original rheological state after 60 min. This process is fully reversible, and the SWCNT-DNA SMHs do not suffer significant damage or alteration following repeated cycling of NIR-triggered sol-gel transitions (Figure 4C). This process also occurs in dilute networks of SWCNT-DNA dispersions that do not gel (Figure S5, Supporting Information), providing additional options for optically triggered solution-based applications.

3. Conclusion

In summary, we have demonstrated stimuli-responsive and reversible SWCNT-DNA SMHs by exploiting noncovalent interactions between SWCNTs and DNA in addition to optimized DNA linker chemistry. Due to the customizable properties of synthetic DNA, further functionality can be straightforwardly introduced to this SMH architecture. The properties of SWCNT-DNA SMHs are also tailorable by varying the SWCNT concentration, particularly allowing enhancement of mechanical properties and integrity. In addition, the SWCNT-DNA SMHs are reversibly responsive to heat, NIR irradiation, and pH, providing a variety of options for dynamically tuning properties via external stimuli. With this unique set of functionalities, SWCNT-DNA SMHs are likely to have broad impact in a variety of applications including sensors, actuators, responsive substrates, and 3D printing.[15]

Experimental Section

Dispersion of SWCNT in DNA: In a four dram vial, equal amounts by weight of SG(6,5) SWCNT powder and $(AC)_{12}S1$ DNA were mixed with duplex buffer (30×10^{-3} M HEPES, 100×10^{-3} M potassium acetate, 1 M NaCl, pH 7.5). The mixture was ultrasonicated for 1 h at a power level of 8–10 W while the vial was cooled in an ice bath. Following ultrasonication, the slurry was centrifuged in 1.5 mL conical Eppendorf tubes to remove aggregates, after which the top 80% was carefully removed with a 20-gauge needle. The resulting dispersion was then dialyzed for a minimum of 3 days in a 100 kDa membrane against duplex buffer, during which the buffer was changed daily.

SWCNT-DNA Gel Synthesis: SWCNTs dispersed in $(AC)_{12}S1$ were mixed with linker DNA in a 1:1 concentration ratio. The mixture was slowly heated in a water bath at a rate of 0.5 °C min^{-1} until it reached 60 °C, after which it was allowed to cool slowly to room temperature at an approximate rate of 0.25 °C min^{-1}.

Molecular Dynamics Simulations: Coarse-grained SWCNTs were modeled through a rigid, linear collection of 280 beads, each with a diameter of $\sigma = 1$ nm (σ is the LJ unit of length). The interbead distance was also 1 nm, so that the length of each SWCNT was 280 nm, which is about 62% of the average length of the SWCNT in experiments (≈450 nm). The S1 strand and $(CG)_n$ strand of linker DNA were modeled using a bead-spring polymer model. It is assumed that the double-stranded DNA formed after hybridization with SWCNT had the B-form, with a pitch distance of 0.332 nm per base pair. Therefore, with a bead size chosen as 1 nm in the simulation, the S1 strand with 12 bases was represented by a polymer chain with 4 beads. Similarly, the $(CG)_n$ strands of the linker DNA with *n* ranging from 2 to 9 corresponded to polymer chains with 1–6 beads. Further experimental and computational details are provided in the Supporting Information.

Supporting Information

Supporting Information is available from the Wiley Online Library or from the author.

Acknowledgements

This work was supported by the National Science Foundation and the Environmental Protection Agency under Cooperative Agreement No. DBI-1266377, and the U.S. Public Health Service Grant No. NIEHS RO1 ES022698. Z.W. and E.L. were also supported by NSF

DMR-1610796. The experimental effort made use of the EPIC facility of the NUANCE Center at Northwestern University, which received support from the NSF Soft and Hybrid Nanotechnology Experimental (SHyNE) Resource (NNCI-1542205); the NSF MRSEC program (DMR-1121262); the International Institute for Nanotechnology (IIN); the Keck Foundation; and the State of Illinois. The authors thank Shay Wallace for photography and Ming Han for providing improved LAMMPS functions to perform dynamic bonding. The authors also acknowledge the Quest high-performance computing facility at Northwestern University for computational resources.

Conflict of Interest

The authors declare no conflict of interest.

Keywords

carbon nanotubes, DNA, near-infrared, optothermally reversible, supramolecular hydrogels

Received: August 28, 2017
Published online:

[1] a) D. Kim, J. Kim, Y. Ko, K. Shim, J. H. Kim, J. You, *ACS Appl. Mater. Interfaces* **2016**, *8*, 33175; b) J. Duan, X. Liang, J. Guo, K. Zhu, L. Zhang, *Adv. Mater.* **2016**, *28*, 8037; c) R. Du, Y. Xu, Y. Luo, X. Zhang, J. Zhang, *Chem. Commun.* **2011**, *47*, 6287; d) C. Li, M. J. Rowland, Y. Shao, T. Cao, C. Chen, H. Jia, X. Zhou, Z. Yang, O. A. Scherman, D. Liu, *Adv. Mater.* **2015**, *27*, 3298; e) B. P. Lee, S. Konst, *Adv. Mater.* **2014**, *26*, 3415; f) H. Wang, S. C. Heilshorn, *Adv. Mater.* **2015**, *27*, 3717; g) C. C. Kim, H. H. Lee, K. H. Oh, J. Y. Sun, *Science* **2016**, *353*, 682.

[2] a) R. Dong, Y. Pang, Y. Su, X. Zhu, *Biomater. Sci.* **2015**, *3*, 937; b) S. Banerjee, R. K. Das, U. Maitra, *J. Mater. Chem.* **2009**, *19*, 6649; c) P. Y. W. Dankers, T. M. Hermans, T. W. Baughman, Y. Kamikawa, R. E. Kieltyka, M. M. C. Bastings, H. M. Janssen, N. A. J. M. Sommerdijk, A. Larsen, M. J. A. Van Luyn, A. W. Bosman, E. R. Popa, G. Fytas, E. W. Meijer, *Adv. Mater.* **2012**, *24*, 2703; d) G. Yu, X. Yan, C. Han, F. Huang, *Chem. Soc. Rev.* **2013**, *42*, 6697; e) J. W. Steed, *Chem. Commun.* **2011**, *47*, 1379.

[3] a) M. Ikeda, T. Tanida, T. Yoshii, I. Hamachi, *Adv. Mater.* **2011**, *23*, 2819; b) E. A. Appel, F. Biedermann, U. Rauwald, S. T. Jones, J. M. Zayed, O. A. Scherman, *J. Am. Chem. Soc.* **2010**, *132*, 14251; c) Y. Shi, M. Wang, C. Ma, Y. Wang, X. Li, G. Yu, *Nano Lett.* **2015**, *15*, 6276; d) S. Roy, A. Baral, A. Banerjee, *Chemistry* **2013**, *19*, 14950; e) J. S. Kahn, A. Trifonov, A. Cecconello, W. Guo, C. Fan, I. Willner, *Nano Lett.* **2015**, *15*, 7773; f) C. B. Rodell, N. N. Dusaj, C. B. Highley, J. A. Burdick, *Adv. Mater.* **2016**, *28*, 8419.

[4] a) D. Jariwala, V. K. Sangwan, L. J. Lauhon, T. J. Marks, M. C. Hersam, *Chem. Soc. Rev.* **2013**, *42*, 2824; b) J. N. Coleman, U. Khan, W. J. Blau, Y. K. Gun'ko, *Carbon* **2006**, *44*, 1624; c) M. I. Sajid, U. Jamshaid, T. Jamshaid, N. Zafar, H. Fessi, A. Elaissari, *Int. J. Pharm.* **2016**, *501*, 278; d) C. Koechlin, S. Maine, R. Haidar, B. Trétout, A. Loiseau, J. L. Pelouard, *Appl. Phys. Lett.* **2010**, *96*, 103501.

[5] a) S. Berciaud, L. Cognet, P. Poulin, R. B. Weisman, B. Lounis, *Nano Lett.* **2007**, *7*, 1203; b) R. B. Weisman, S. M. Bachilo, *Nano Lett.* **2003**, *3*, 1235; c) T. L. Troy, S. N. Thennadil, *J. Biomed. Opt.* **2001**, *6*, 167.

[6] a) J. T. Seo, N. L. Yoder, T. A. Shastry, J. J. Humes, J. E. Johns, A. A. Green, M. C. Hersam, *J. Phys. Chem. Lett.* **2013**, *4*, 2805; b) R. Yang, Z. Tang, J. Yan, H. Kang, Y. Kim, Z. Zhu, W. Tan, *Anal. Chem.* **2008**, *80*, 7408; c) M. Zheng, A. Jagota, E. D. Semke, B. A. Diner, R. S. McLean, S. R. Lustig, R. E. Richardson, N. G. Tassi, *Nat. Mater.* **2003**, *2*, 338.

[7] a) X. Zhang, C. L. Pint, M. H. Lee, B. E. Schubert, A. Jamshidi, K. Takei, H. Ko, A. Gillies, R. Bardhan, J. J. Urban, M. Wu, R. Fearing, A. Javey, *Nano Lett.* **2011**, *11*, 3239; b) S. R. Shin, H. Bae, J. M. Cha, J. Y. Mun, Y. C. Chen, H. Tekin, H. Shin, S. Farshchi, M. R. Dokmeci, S. Tang, A. Khademhosseini, *ACS Nano* **2012**, *6*, 362; c) T. Fujigaya, T. Morimoto, Y. Niidome, N. Nakashima, *Adv. Mater.* **2008**, *20*, 3610; d) E. Miyako, H. Nagata, K. Hirano, T. Hirotsu, *Small* **2008**, *4*, 1711; e) L. Y. Yan, H. Chen, P. Li, D. H. Kim, M. B. Chan-Park, *ACS Appl. Mater. Interfaces* **2012**, *4*, 4610.

[8] a) T. Fukushima, A. Kosaka, Y. Ishimura, T. Yamamoto, T. Takigawa, N. Ishii, T. Aida, *Science* **2003**, *300*, 2072; b) K. H. Kim, Y. Oh, M. F. Islam, *Nat. Nanotechnol.* **2012**, *7*, 562.

[9] a) Z. Tan, S. Ohara, M. Naito, H. Abe, *Adv. Mater.* **2011**, *23*, 4053; b) Z. Wang, Y. Chen, *Macromolecules* **2007**, *40*, 3402.

[10] a) T. Ogoshi, Y. Takashima, H. Yamaguchi, A. Harada, *J. Am. Chem. Soc.* **2007**, *129*, 4878; b) Y. Z. You, J. J. Yan, Z. Q. Yu, M. M. Cui, C. Y. Hong, B. J. Qu, *J. Mater. Chem.* **2009**, *19*, 7656; c) E. Cheng, Y. Li, Z. Yang, Z. Deng, D. Liu, *Chem. Commun.* **2011**, *47*, 5545; d) S. Tamesue, Y. Takashima, H. Yamaguchi, S. Shinkai, A. Harada, *Eur. J. Org. Chem.* **2011**, *2011*, 2801; e) G. N. Ostojic, M. C. Hersam, *Small* **2012**, *8*, 1840; f) R. Du, J. Wu, L. Chen, H. Huang, X. Zhang, J. Zhang, *Small* **2014**, *10*, 1387.

[11] a) Y. Zeng, J. Q. Lu, *ACS Nano* **2014**, *8*, 11695; b) T. Jungst, W. Smolan, K. Schacht, T. Scheibel, J. Groll, *Chem. Rev.* **2016**, *116*, 1496.

[12] a) C. A. Mirkin, R. L. Letsinger, R. C. Mucic, J. J. Storhoff, *Nature* **1996**, *382*, 607; b) S. Y. Park, A. K. R. Lytton-Jean, B. Lee, S. Weigand, G. C. Schatz, C. A. Mirkin, *Nature* **2008**, *451*, 553; c) A. K. R. Lytton-Jean, C. A. Mirkin, *J. Am. Chem. Soc.* **2005**, *127*, 12754; d) J. S. Lee, A. K. R. Lytton-Jean, S. J. Hurst, C. A. Mirkin, *Nano Lett.* **2007**, *7*, 2112.

[13] A. Shankar, J. Mittal, A. Jagota, *Langmuir* **2014**, *30*, 3176.

[14] a) K. J. Breslauer, R. Frank, H. Blöcker, L. A. Marky, *Proc. Natl. Acad. Sci. USA* **1986**, *83*, 3746; b) J. SantaLucia, *Proc. Natl. Acad. Sci. USA* **1998**, *95*, 1460.

[15] Y. Xu, P. E. Pehrsson, L. Chen, R. Zhang, W. Zhao, *J. Phys. Chem. C* **2007**, *111*, 8638.

